Materials Transactions, Vol. 51, No. 6 (2010) pp. 1168 to 1172

EXPRESS REGULAR ARTICLE

Formation of Hägg Carbide in an Fe-30Mn-10Al-4Cr-0.45C Alloy

YiHsuan Tuan*[1], ChuenGuang Chao and TzengFeng Liu*[2]

Department of Materials Science and Engineering, National Chiao Tung University, 1001 Ta Hsueh Road, Hsinchu 30049, Taiwan, R. O. China

When the present alloy was aged at 550°C, Hägg carbides (M_5C_2-type carbides) formed at a/2⟨100⟩ anti-phase boundaries of the $D0_3$ domains. The Hägg carbide has never been observed by previous workers in FeMnAlC and FeMnAlCrC alloy systems. The orientation relationship between Hägg carbide and $D0_3$ matrix was determined to be $(\bar{5}10)_{M_5C_2}$ // $(1\bar{1}0)_{D0_3}$ and $(13\bar{4})_{M_5C_2}$ // $(10\bar{2})_{D0_3}$. The orientation relationship between Hägg carbide and bcc-type phase has also never been reported before. [doi:10.2320/matertrans.M2010055]

(Received February 12, 2010; Accepted March 24, 2010; Published April 28, 2010)

Keywords: *alloys, transmission electron microscope (TEM), electron diffraction, microstructure, Hägg carbide*

1. Introduction

In previous studies,[1–6] it is seen that the as-quenched microstructure of the Fe-(28–34)mass%Mn-(7.8–11)mass%Al-(0.54–1.3)mass%C alloys was single-phase austenite (γ). After being aged at 500–750°C for moderate times, fine and coarse $(Fe,Mn)_3AlC$ carbides were found to precipitate coherently within the γ matrix and heterogeneously on the γ/γ grain boundaries, respectively. For convenience, the κ' carbide and κ carbide were used to represent the $(Fe,Mn)_3AlC$ carbide formed coherently within the γ matrix and heterogeneously on the γ/γ grain boundaries.[2] After prolonged aging time within this temperature range, the coarse κ carbides grew into adjacent γ grains through a $\gamma \rightarrow \alpha$(ferrite) + β-Mn reaction, a $\gamma \rightarrow \gamma_0$(carbon-deficient austenite) + κ reaction, a $\gamma \rightarrow \beta$-Mn + κ reaction or a $\gamma \rightarrow \alpha + \beta$-Mn + κ reaction,[1–5] depending on the chemical composition and aging temperature. In the FeMnAlC alloys with lower carbon content (i.e. 0.4–0.51 mass%C), the as-quenched microstructure was found to be $(\gamma + \alpha)$ dual phases.[7–9] After being aged at 550–710°C, fine κ' carbides were found to appear within the γ grains, and coarse κ carbides as well as β-Mn precipitates could be observed in the α grains and on the α/α grain boundaries.[8,9] In 1991, the present workers examined the microstructural developments of an Fe-28.6 mass%Mn-10.1 mass%Al-0.46 mass%C alloy.[10] Consequently, it was found that in the as-quenched condition, extremely fine $D0_3$ domains could be observed within the α grains. This is different from that reported by other workers in the duplex FeMnAlC alloys. When the alloy was aged at temperatures ranging from 450 to 750°C, the phase transformation sequence occurring within the α grain was found to be $\alpha + D0_3 \rightarrow \alpha + D0_3 + \kappa \rightarrow \alpha + B2 + \kappa \rightarrow \alpha$.[10]

In order to improve the corrosion resistance and high-temperature oxidation resistance, the Cr has been added to the austenitic or duplex FeMnAlC alloys.[11–15] Based on these results, it can be generally concluded that the addition of Cr does achieve these results. Additionally, the effects of Cr addition on the microstructures of the austenitic FeMnAlC alloys have also been examined by several researchers.[16,17] In the previous study,[16] it is seen that when the Fe-30 mass%Mn-9 mass%Al-5 mass%Cr-0.7 mass%C alloy was aged at 550–750°C, the fine κ' carbides were formed within the γ grain, and a $(M_7C_3 + D0_3) \rightarrow (M_7C_3 + B2) \rightarrow (M_7C_3 + \alpha)$ reaction occurred on the γ/γ grain boundaries. Besides, when the Fe-28.3 mass%Mn-8.7 mass%Al-5.5 mass%Cr-1 mass%C alloy was aged at 800–1250°C, a $(\gamma + Cr_7C_3) \rightarrow \gamma \rightarrow (\gamma + (\alpha + B2 + D0_3))$ reaction occurred within the γ grain and on the γ/γ grain boundaries.[17] In contrast to the studies of the austenitic FeMnAlCrC alloys, information concerning the microstructures of the $(\gamma + \alpha)$ duplex FeMnAlCrC alloys is very deficient. Therefore, the purpose of this work is an attempt to study the microstructural developments in the Fe-30 mass%Mn-10 mass%Al-4 mass%Cr-0.45 mass%C alloy aged at 550°C.

2. Experimental Procedure

The Fe-30 mass%Mn-10 mass%Al-4 mass%Cr-0.45 mass%C alloy was prepared in a vacuum induction furnace using pure Fe, Mn, Al, Cr and carbon powder. After being homogenized at 1250°C for 12 h, the ingot was hot-rolled to a final thickness of 2.0 mm. The sheet was subsequently solution heat-treated (SHT) at 1050°C for 1 h and then rapidly quenched into room-temperature water. Aging process was performed at 550°C for 12 h in a vacuum furnace followed by rapid quenching. Electron microscopy specimens were prepared by means of a double-jet electropolisher with an electrolyte of 65% ethanol, 20% acetic acid and 15% perchloric acid. Electron microscopy was performed on a JEOL 2100 transmission electron microscope (TEM) operating at 200 kV. This microscope was equipped with a Link ISIS 300 energy-dispersive X-ray spectrometer (EDS) for chemical analysis. Quantitative analyses of elemental concentrations for Fe, Mn, Al and Cr were made using the Cliff-Lorimer ratio thin section method. The EDS with a thick-window detector is limited to detect the elements of atomic number of 11 or above. Therefore, carbon cannot be examined by this method.

*[1]Graduate Student, National Chiao Tung University

*[2]Corresponding author, E-mail: tfliu@cc.nctu.edu.tw; yixduan.mse89g@nctu.edu.tw

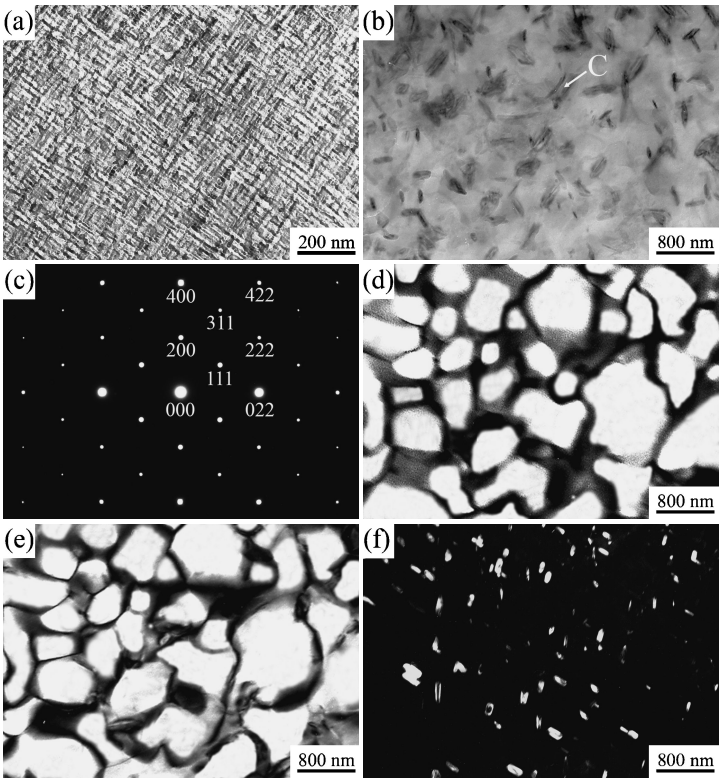

Fig. 1 Transmission electron micrographs of the alloy aged at 550°C for 12 h. (a) BF taken from the γ matrix; (b)–(f) taken from the $D0_3$ matrix. (b) BF, (c) an SADP, the zone axis is $[01\bar{1}]$, (d) and (e) (111) and (200) $D0_3$ DF image, respectively, (f) $(001)_{M_5C_2}$ DF image.

3. Results and Discussion

In the as-quenched condition, the microstructure of the alloy was $(\gamma + \alpha)$ dual phases. No precipitates could be detected within the γ grains; however, extremely fine $D0_3$ domains could be observed within the α grains. The extremely fine $D0_3$ domains were formed within the α grains by a continuous ordering transition during quenching. This is similar to that observed by the present workers in the Fe-28.6 mass%Mn-10.1 mass%Al-0.46 mass%C alloy.[10] When the as-quenched alloy was aged at 550°C for 12 h, fine k′ carbides were formed within the γ grain, as shown in Fig. 1(a). Figure 1(b) is a bright-field (BF) electron micrograph taken from the α grain, indicating that a lot of small precipitates occurred within the α matrix. Figure 1(c) is a selected-area diffraction pattern (SADP) taken from the α matrix, exhibiting the presence of the superlattice reflection spots of the ordered $D0_3$ phase.[10] Figures 1(d) and (e) are the (111) and (200) $D0_3$ dark-field (DF) electron micrographs taken from the same area as Fig. 1(b), clearly revealing that the (111) DF image and the (200) DF image are morphologically identical. Therefore, the bright domains presented in Figs. 1(d) and (e) are of the $D0_3$ phase with $a/2\langle 100\rangle$ antiphase boundaries (APBs).[10] Figure 1(f) is the DF image of the small precipitates, indicating that these precipitates have occurred preferentially at $a/2\langle 100\rangle$ APBs of the $D0_3$ domains. A preliminary study of electron diffraction indicated that the precipitate was not of any known phases reported in FeMnAl, FeMnAlC and FeMnAlCrC alloy systems.[1–17] In order to clarify the crystal structure of the precipitate, eight SADPs taken from the precipitate marked as C in Fig. 1(b) were obtained by tilting the specimen about some specific reflections. The results are shown in Figs. 2(a)–(h). Table 1(a) shows the interplanar spacings of the precipitate phase, which were measured directly from the SADPs in Figs. 2(a)–(h). The measured angles among the reciprocal lattice vectors are listed in Table 1(b). Using these measured values of the interplanar spacings and angles, the crystal structure of the precipitate was determined to be monoclinic with lattice parameters $a = 1.158$ nm, $b = 0.452$ nm, $c = 0.509$ nm, and $\beta = 98.3°$. Based on these lattice parameters, the interplanar spacings and the angles between the chosen reciprocal reflections were calculated by using the following equations:[18]

$$\frac{1}{d^2} = \frac{1}{a^2}\frac{h^2}{\sin^2\beta} + \frac{1}{b^2}k^2 + \frac{1}{c^2}\frac{l^2}{\sin^2\beta} - \frac{2hl\cos\beta}{ac\sin^2\beta}$$

$$\cos\phi = \frac{\dfrac{1}{a^2}h_1h_2 + \dfrac{1}{b^2}k_1k_2\sin^2\beta + \dfrac{1}{c^2}l_1l_2 - \dfrac{1}{ac}(l_1h_2 + l_2h_1)\cos\beta}{\left\{\left(\dfrac{1}{a^2}h_1^2 + \dfrac{1}{b^2}k_1^2\sin^2\beta + \dfrac{1}{c^2}l_1^2 - \dfrac{2h_1l_1}{ac}\cos\beta\right) \times \left(\dfrac{1}{a^2}h_2^2 + \dfrac{1}{b^2}k_2^2\sin^2\beta + \dfrac{1}{c^2}l_2^2 - \dfrac{2h_2l_2}{ac}\cos\beta\right)\right\}^{1/2}}$$

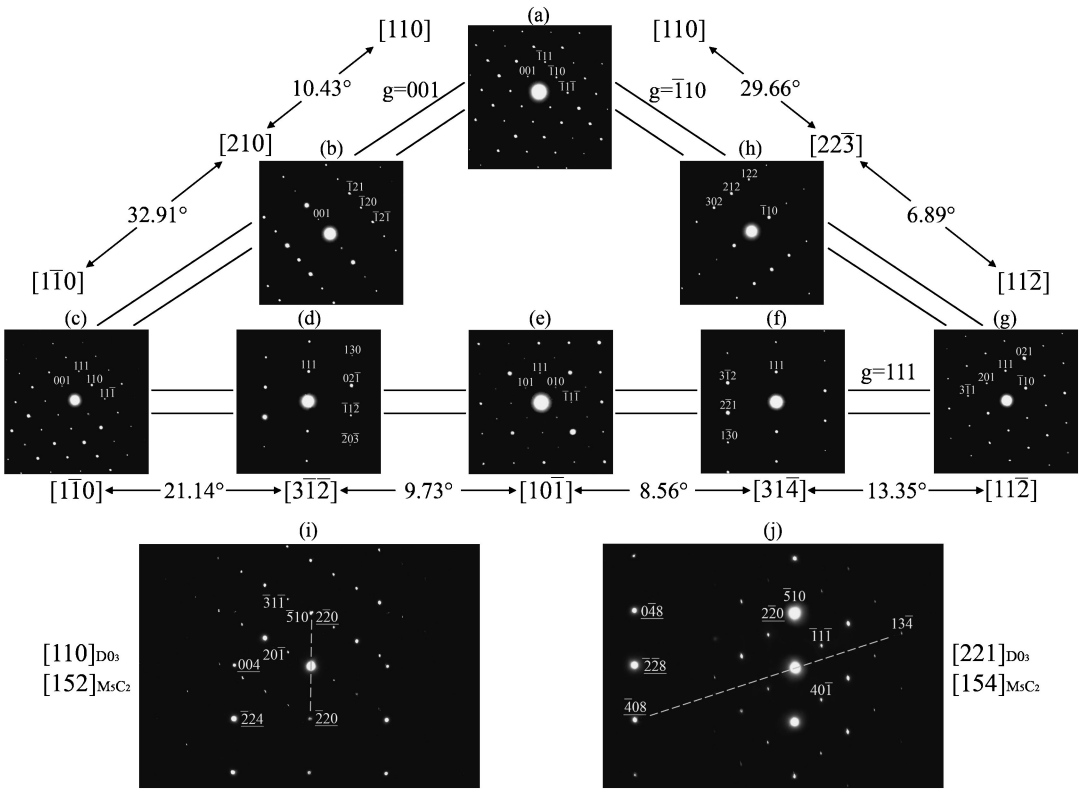

Fig. 2 (a–h) Eight SADPs taken from the precipitate marked "C" in Fig. 1(b). The zone axes are (a) [110], (b) [210], (c) [1$\bar{1}$0], (d) [3$\bar{1}\bar{2}$], (e) [10$\bar{1}$], (f) [31$\bar{4}$], (g) [11$\bar{2}$] and (h) [22$\bar{3}$], respectively. (i) and (j) Two SADPs taken from an area including the precipitate marked "C" and its surrounding matrix in Fig. 1(b). The zone axes are (i) $[152]_{M_5C_2}$, $[110]_{D0_3}$ and (j) $[154]_{M_5C_2}$, $[221]_{D0_3}$, respectively. (hkl = M_5C_2 carbide; $\underline{hkl}$ = $D0_3$ phase)

The calculated interplanar spacings and angles are also listed in Table 1 for comparison. It is seen in Table 1 that the measured values are quite consistent with those obtained by calculation. Therefore, the SADPs of the precipitate phase in Figs. 2(a)–(h) could all be indexed. The zone axes of Figs. 2(a)–(h) are [110], [210], [1$\bar{1}$0], [3$\bar{1}\bar{2}$], [10$\bar{1}$], [31$\bar{4}$], [11$\bar{2}$] and [22$\bar{3}$], respectively. Compared with previous studies,[19–23] it is clear that the crystal structure of the precipitate corresponds to that of the Hägg carbide (M_5C_2-type carbide).

Based on the preceding observations, two important experimental results are discussed below. (I) The coarse Mn-rich κ carbides or Mn-rich β-Mn precipitates were always observed within the α or $D0_3$ matrix in the duplex FeMnAlC alloys aged at 450–750°C.[8–10] However, only M_5C_2 carbides were formed at a/2⟨100⟩ APBs of the well-grown $D0_3$ domains, and no evidence of κ carbide or β-Mn precipitate could be detected within the α grain in the present alloy aged at 550°C. In order to clarify the apparent difference, an TEM-EDS study was made. The average concentrations of the alloying elements were obtained from at least ten different EDS profiles of each phase. The results are summarized in Table 2. It is seen in Table 2 that the Cr and Mn concentrations in the well-grown $D0_3$ domains were much lower than those in the as-quenched alloy, and the reverse result was obtained in the M_5C_2 carbide. Therefore, it is believed that during the growth of the $D0_3$ domains, partial Cr and Mn atoms would proceed to diffuse toward the a/2⟨100⟩ APBs. The higher concentrations of both Cr and Mn would cause the (Cr,Mn)-rich M_5C_2 carbides to precipitate at a/2⟨100⟩ APBs. The precipitation of the (Cr,Mn)-rich M_5C_2 carbides would decrease the Mn concentration drastically, thus inhibiting the precipitation of both Mn-rich κ carbides and Mn-rich β-Mn precipitates within the α grain. (II) The Hägg carbide was extensively observed by many workers in the bcc-type alloys.[20–24] Depending on the chemical compositions, the lattice parameters of the Hägg carbide varied in the range of $a = 1.150$–1.158 nm, $b = 0.452$–0.457 nm, $c = 0.501$–0.509 nm and $\beta = 97.6$–$98.3°$.[19–22] However, to date, the orientation relationship between the Hägg carbide and the bcc-type (i.e. α, $D0_3$, B2) structure is very deficient. We are aware of two articles,[22,23] in which they reported that both Fe_5C_2 carbide and Fe_3C carbide were formed intimately in α-iron after being heat-treated at 500–800°C under a CO or/and H_2 atmosphere. By using electron diffraction, the orientation relationship between the Fe_5C_2 and Fe_3C was determined to be $(100)_{Fe_5C_2}$ // $(001)_{Fe_3C}$.[22,23] In addition, they correlated the obtained result with the orientation relationship between Fe_3C and α phase, $(001)_{Fe_3C}$ // $(211)_\alpha$, which was reported by other workers in ferritic stainless steel.[24] Therefore, they deduced that the orientation relationship among Fe_5C_2, Fe_3C and α phase was $(100)_{Fe_5C_2}$ // $(001)_{Fe_3C}$ // $(211)_\alpha$.[23] It is well-known that the orientation relationship between two phases should be described by a pair of parallel directions in a pair of parallel planes or two pairs of parallel planes. However, in the previous studies,[22,23] only a pair of parallel planes was determined and no direct experiment evidence confirmed the orientation relationship between

Table 1 (a) The d spacings of the Hägg carbide. (b) Angles among some reciprocal vectors of the Hägg carbide.

(a) The d Spacings of the Hägg Carbide (nm)				(b) Angles among Some Reciprocal Vectors of the Hägg Carbide (Deg)			
	Observed d Spacing*1	Calculated d Spacing*2	Indexed Plane		Two Desired Reciprocal Vectors	Observed Angle*1	Calculated Angle*2
1	0.504	0.504	001	Fig. 2(a)	(001) and $(\bar{1}11)$	51.8	51.9
2	0.452	0.452	010		(001) and $(\bar{1}10)$	93.1	93.0
3	0.437	0.438	101		(001) and $(\bar{1}1\bar{1})$	131.5	131.6
4	0.418	0.420	$\bar{1}10$	Fig. 2(b)	(001) and $(\bar{1}21)$	67.5	67.6
5	0.419	0.420	110		(001) and $(\bar{1}20)$	91.4	91.6
6	0.315	0.315	111		(001) and $(\bar{1}2\bar{1})$	115.0	115.1
7	0.331	0.332	$\bar{1}11$	Fig. 2(c)	(001) and (111)	48.5	48.4
8	0.330	0.332	$11\bar{1}$		(001) and (110)	87.0	87.0
9	0.316	0.315	$1\bar{1}1$		(001) and $(11\bar{1})$	128.3	128.1
10	0.208	0.206	$02\bar{1}$	Fig. 2(d)	(111) and $(02\bar{1})$	68.5	68.7
11	0.220	0.222	$\bar{1}20$		(111) and $(\bar{1}1\bar{2})$	107.5	107.4
12	0.352	0.354	201		(111) and $(\bar{2}0\bar{3})$	135.7	135.5
13	0.411	0.409	$20\bar{1}$	Fig. 2(e)	(111) and (101)	44.3	44.1
14	0.213	0.211	$\bar{1}1\bar{2}$		(111) and (010)	45.8	45.9
15	0.206	0.205	$\bar{1}21$		(111) and $(\bar{1}1\bar{1})$	91.6	91.8
16	0.203	0.201	$\bar{1}2\bar{1}$	Fig. 2(f)	(111) and $(3\bar{1}2)$	68.3	68.2
17	0.367	0.364	122		(111) and $(2\bar{2}1)$	102.5	102.4
18	0.195	0.197	212		(111) and $(1\bar{3}0)$	130.2	130.0
19	0.193	0.190	$2\bar{2}1$	Fig. 2(g)	(111) and $(\bar{1}10)$	59.0	59.1
20	0.145	0.149	$1\bar{3}0$		(111) and (204)	45.3	45.1
21	0.238	0.241	$3\bar{1}1$		(111) and $(3\bar{1}1)$	79.6	79.8
22	0.159	0.155	$\bar{2}0\bar{3}$	Fig. 2(h)	$(\bar{1}10)$ and (122)	53.8	53.9
23	0.197	0.198	302		$(\bar{1}10)$ and (212)	76.4	76.2
24	0.180	0.181	$3\bar{1}2$		$(\bar{1}10)$ and (302)	103.5	103.4
25	0.268	0.266	$40\bar{1}$	Fig. 2(i)	$(20\bar{1})$ and $(\bar{3}1\bar{1})$	92.1	92.1
26	0.099	0.097	$13\bar{4}$		$(20\bar{1})$ and $(\bar{5}10)$	122.0	122.1
27	2.048	2.044	$\bar{5}10$	Fig. 2(j)	$(\bar{1}1\bar{1})$ and $(40\bar{1})$	89.5	89.3
					$(\bar{1}1\bar{1})$ and $(13\bar{4})$	21.5	21.4
					$(\bar{1}1\bar{1})$ and $(\bar{5}10)$	50.3	50.2

*1The observed d spacings and angles were measured from SADPs.

*2The calculated d spacings and angles were obtained on the basis of the monoclinic structure with lattice parameters $a = 1.158$ nm, $b = 0.452$ nm, $c = 0.509$ nm and $\beta = 98.3$ deg.

Table 2 Chemical compositions of the phases revealed by EDS.

Heat Treatment	Phase	Chemical Composition (at%)			
		Fe	Mn	Al	Cr
SHT	γ	49.07	30.20	17.05	3.68
	$\alpha + D0_3$	52.07	21.80	21.55	4.58
550°C, 12 h	$D0_3$	57.56	16.32	25.18	0.94
	M_5C_2	30.56	43.20	1.02	25.22

Fe_5C_2 and α phase. Therefore, the electron diffraction technique was used to clarify the orientation relationship between the M_5C_2 carbide and the $D0_3$ matrix in the present study. The results are presented in Figs. 2(i) and (j). In these two SADPs, it is clear that the $(\bar{5}10)$ and $(13\bar{4})$ reflection spots of the M_5C_2 carbide are parallel to the $(1\bar{1}0)$ and $(\bar{1}02)$ reflection spots of the $D0_3$ matrix, respectively. Accordingly, the orientation relationship between the M_5C_2 carbide and $D0_3$ matrix can be stated as follows: $(\bar{5}10)_{M_5C_2} // (1\bar{1}0)_{D0_3}$ and $(13\bar{4})_{M_5C_2} // (10\bar{2})_{D0_3}$. In order to further certify the determined orientation relationship, the angle between the $(\bar{5}10)_{M_5C_2}$ and $(13\bar{4})_{M_5C_2}$ was calculated by using the equation mentioned above. The calculated angle was 71.61°, which is quite consistent with the angle of 71.57° between the $(1\bar{1}0)_{D0_3}$ and $(10\bar{2})_{D0_3}$. Finally, it is worth mentioning that in the present study, a lot of effort was made to determine the parallel relationship of lower index planes between the M_5C_2 carbide and $D0_3$ matrix. Unfortunately, the attempt was not successful.

4. Conclusions

In summary, the as-quenched microstructure of the Fe-30 mass%Mn-10 mass%Al-4 mass%Cr-0.45 mass%C alloy was $(\gamma + \alpha)$ dual phases, and extremely fine $D0_3$ domains could be observed within the α grains. After being aged at 550°C for 12 h, fine κ' carbides were formed within the γ grains and the (Cr,Mn)-rich Hägg carbides occurred at $a/2\langle 100\rangle$ APBs of the well-grown $D0_3$ domains. The Hägg carbide has never been observed by previous workers in FeMnAlC and FeMnAlCrC alloy systems. The orientation relationship between the Hägg carbide and $D0_3$ matrix was

determined to be $(\bar{5}10)_{M_5C_2}$ // $(1\bar{1}0)_{D0_3}$ and $(13\bar{4})_{M_5C_2}$ // $(10\bar{2})_{D0_3}$. The orientation relationship between Hägg carbide and bcc-type phase has also never been reported by other workers before.

Acknowledgments

This project was supported by the National Science Council, Taiwan (NSC-97-2221-E-009-027-MY3).

REFERENCES

1) K. Sato, K. Tagawa and Y. Inoue: Metall. Trans. A **21A** (1990) 5–11.
2) W. K. Choo, J. H. Kim and J. C. Yoon: Acta Mater. **45** (1997) 4877–4885.
3) C. Y. Chao, C. N. Hwang and T. F. Liu: Scr. Metall. **28** (1993) 109–114.
4) G. S. Krivonogov, M. F. Alekseyenko and G. G. Solovyeva: Fiz. Metal. Metalloved **39** (1975) 775–781.
5) C. N. Hwang, C. Y. Chao and T. F. Liu: Scr. Metall. **28** (1993) 263–268.
6) T. F. Liu, J. S. Chou and C. C. Wu: Metall. Trans. A **21A** (1990) 1891–1899.
7) S. C. Tjong and S. M. Zhu: Mater. Trans. JIM **38** (1997) 112–118.
8) S. C. Tjong and N. J. Ho: Metallography **21** (1988) 199–206.
9) T. F. Liu and C. M. Wan: Strength Met. Alloys **1** (1986) 423–428.
10) C. C. Wu, J. S. Chou and T. F. Liu: Metall. Trans. A **22A** (1991) 2265–2276.
11) C. S. Wang, C. Y. Tsai, C. G. Chao and T. F. Liu: Mater. Trans. **48** (2007) 2973–2977.
12) Y. H. Tuan, C. S. Wang, C. Y. Tsai, C. G. Chao and T. F. Liu: Mater. Chem. Phys. **114** (2009) 595–598.
13) S. C. Chang, W. H. Weng, H. C. Chen, S. J. Lin and P. C. K. Chung: Wear **181–183** (1995) 511–515.
14) C. J. Wang and Y. C. Chang: Mater. Chem. Phys. **76** (2002) 151–161.
15) J. G. Duh and C. J. Wang: J. Mater. Sci. **25** (1990) 268–276.
16) Y. H. Tuan, C. L. Lin, C. G. Chao and T. F. Liu: Mater. Trans. **49** (2008) 1589–1593.
17) C. M. Liu, H. C. Cheng, C. Y. Chao and K. L. Ou: J. Alloy. Compd. **488** (2009) 52–56.
18) J. W. Edington: *Practical Electron Microscopy in Materials Science*, (Van Nostrand Reinhold Company, New York, 1976) pp. 281–291.
19) F. Ernst, Y. Cao and G. M. Michal: Acta Mater. **52** (2004) 1469–1477.
20) H. I. Faraoun, Y. D. Zhang, C. Esling and H. Aourag: J. Appl. Phys. **99** (2006) 093508-1–090358-8.
21) E. Bauer-Grosse, C. Frantz and G. Lecaer: J. Non-Cryst. Solids **44** (1981) 277–286.
22) V. D. Blank, Y. L. Alshevskiy, A. I. Zaitsev, N. V. Kazennov, I. A. Perezhogin and B. A. Kulnitskiy: Scr. Mater. **55** (2006) 1035–1038.
23) M. Audier, P. Bowen and W. Jones: J. Cryst. Growth **64** (1983) 291–296.
24) X. Huang and N. H. Pryds: Acta Mater. **48** (2000) 4073–4082.